Journal of Electroceramics, 10, 83–88, 2003
© 2003 Kluwer Academic Publishers. Manufactured in The Netherlands.

Characteristics of Textured Ce-Zr Mixed-Oxide Films as Buffer Layer for YBCO Coated Conductors

H.Y. LEE, S.I. KIM, Y.C. LEE, Y.P. HONG, Y.H. PARK & K.H. KO

Department of Materials Science & Engineering, Ajou University, Suwon, 442-749, South Korea

Submitted November 12, 2002; Revised January 30, 2003; Accepted March 20, 2003

Abstract. Single- and multi-layer $(Ce_{1-x}Zr_x)O_2$ films ($0 \leq x \leq 0.84$) on Si (100) and polycrystalline Ni substrates were prepared using RF and DC magnetron co-sputtering. XRD of ϕ scan analysis showed that all $(Ce_{1-x}Zr_x)O_2$ films were biaxially oriented with the *c*-axis perpendicular to the plane of the film. During sputtering, DC power to the Zr target was fixed at 200 W, while RF power to the Ce target was set at 30 W, 50 W, or 100 W. As-deposited ZrO_2 film was amorphous and was crystallized by post-annealing. However, as-deposited $(Ce_{1-x}Zr_x)O_2$ films were crystalline even when grown at room temperature and the structures of films were cubic or tetragonal depending on the Ce ion incorporation. It was found that multilayered $CeO_2/(Ce_{1-x}Zr_x)O_2/CeO_2$ films could be deposited with a continuous compositional gradient in a sputtering batch. This layered CeO_2/CZO/CeO_2 structure can maintain its original texture after 800°C annealing and is therefore suitable for subsequent YBCO film growth. Furthermore, Ni diffusion is effectively blocked by the buffer layers just like the YSZ currently used in coated conductor fabrication.

Keywords: magnetron co-sputtering, compositional gradient, $(Ce_{1-x}Zr_x)O_2$ films

1. Introduction

Buffer layers for high T_c superconductor films have been widely employed to prevent chemical interaction between substrates and high T_c superconductor films [1, 2]. In the case of $YBa_2Cu_3O_{7-x}$ coated conductor films, CeO_2 films are used for seed layers as well as cap layers owing to their good lattice and thermal matching with YBCO films, while YSZ film is used between the ceria layers as diffusion barrier to block contamination from the substrate [3–5]. High quality buffer films have been obtained by various methods, such as PLD (Pulsed Laser Deposition), E-beam evaporation, MOCVD (Metal Organic Chemical Vapor Deposition), Magnetron sputtering, IBAD (Ion Beam Assisted Deposition). In 1991, biaxially aligned YSZ films were successfully deposited by Iijima et al. on a polycrystalline Ni-based alloy and on fused silica substrates by IBAD. Further work at Los Alamos National Laboratory (LANL) has optimized these processes to yield excellent results [6, 7]. Recently, it was reported that $Ce_{1-x}La_xO_{2-x/2}$ and $Zr_{1-x}Ce_xO_2$ film deposited by PLD might also serve as effective buffer layers [8]. In order to utilize such varied materials in multi-layer superconductor architectures, it is very important to obtain high quality interfaces between seed/substrate, cap/diffusion barrier, seed/diffusion, and cap/YBCO film.

It has been reported that ceria (CeO_2) can stabilize zirconia with cubic or tetragonal phases just like yttria (Y_2O_3) [9–12]. According to Rossignol [9], $(Ce_x Zr_{1-x})O_2$ has a tetragonal structure for $0 \leq x \leq 0.16$, while for $0.16 \leq x \leq 1$, it forms both cubic and tetragonal phases in bulk materials. Therefore, by simply changing the composition from $x = 0$ to other values, it was possible to deposit a sophisticated structure of successive buffer layers, e.g. CeO(seed)/$(Ce_{1-x}Zr_x)O_2$ (diffusion barrier)/CeO_2(cap) in one batch process. Furthermore, enhanced lattice and thermal expansion matching can be expected due to minimized interfacial disruption by gradual composition changes from seed to cap. In this study, a reactive sputtering system with two metallic targets of simple metallic composition was used. All buffer layers were deposited successively and

the properties of $(Ce_{1-x}Zr_x)O_2$ films were investigated as a buffer layer for YBCO coated conductors.

2. Experimental Procedure

Crystalline, textured $(Ce_{1-x}Zr_x)O_2$ films were deposited by RF and DC magnetron sputtering at ambient temperature, using an incident angle of about 50° to the normal of the film plane between substrate and target. The distances between targets (Zr, Ce) and substrate were 13 cm and 8 cm, respectively. A schematic drawing of the set-up for the film deposition is given in Fig. 1. For Si (100) substrate cleaning, Si (100) substrates were treated with a diluted HF solution (HF : DI water = 1 : 10) to remove native SiO_2 on the surfaces, and the substrates were rinsed in deionized water. Ultrasonic treatment with trichloroethylene and acetone was also used to remove organics. The depositions were made in a high vacuum system with a base pressure of 3×10^{-6} Torr. The Ce metal and Zr metal target were disks with diameters of 2 inches (99.9%) and 4 inches (99.9%), respectively. Each target was pre-sputtered with pure Ar for 30 minutes before deposition to remove any target oxidation formed during previous run. The plasma was generated from pure Ar gas and an additional flow of Ar/O_2 mixture (10:1 by volume) was used during deposition to maintain 10 mTorr of total pressure. The DC power of the Zr target was fixed at 200 W, while the RF power of the Ce target was changed from 30 W to 100 W. Some of the as-deposited $(Ce_{1-x}Zr_x)O_2$ films were annealed in air at 800°C for 3 hours. The structure of the films was characterized by Cu Kα x-rays diffraction (XRD, Mac Science M18XHF, Japan) and the in-plane orientation of the films was analyzed by ϕ scan XRD (Rigaku DMAX PSPC MDG 2000, Japan). The electronic state of the Ce atoms on the surface was analyzed by x-ray photoelectron spectroscopy (XPS; Ariesarsc 16MCD150, Vacuum Science Workshop, United Kingdom). In addition, the surface morphology of the films was investigated by scanning electron microscopy (SEM, JEOL JSM-6330F) equipped with

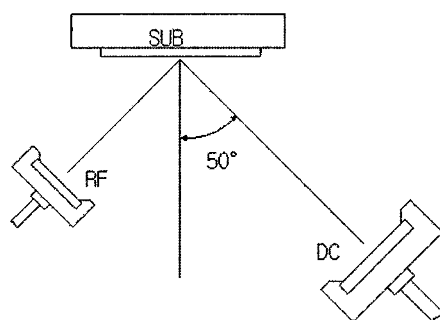

Fig. 1. The schematic diagram of the sputtering apparatus used in this work: (a) Ce metal and (b) Zr metal.

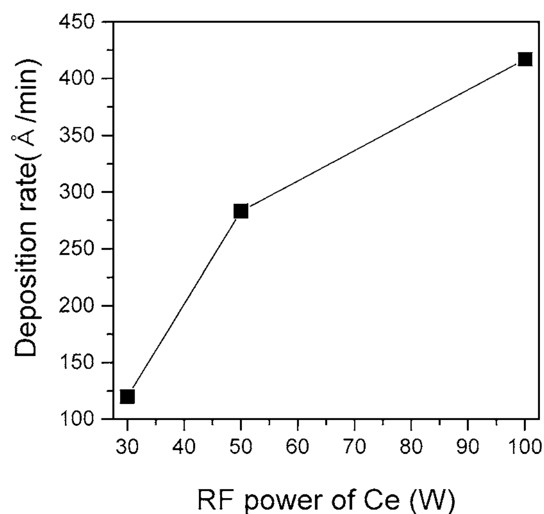

Fig. 2. The deposition rate of $(Ce_{1-x}Zr_x)O_2$ films with increasing RF power of Ce.

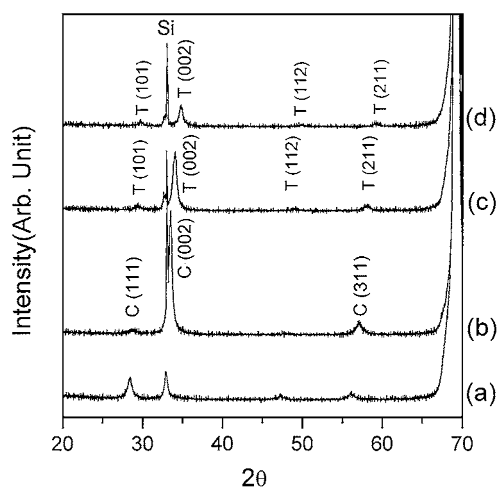

Fig. 3. XRD patterns of as-deposited CeO_2 film and $(Ce_{1-x}Zr_x)O_2$ films deposited with different RF power of Ce: (a) as-deposited CeO_2 film (Ce power of 100 W), (b) $(Ce_{0.75}Zr_{0.25})O_2$ film (Ce power of 100 W), (c) $(Ce_{0.5}Zr_{0.5})O_2$ film (Ce power of 50 W), and (d) $(Ce_{0.16}Zr_{0.84})O_2$ film (Ce power of 30 W).

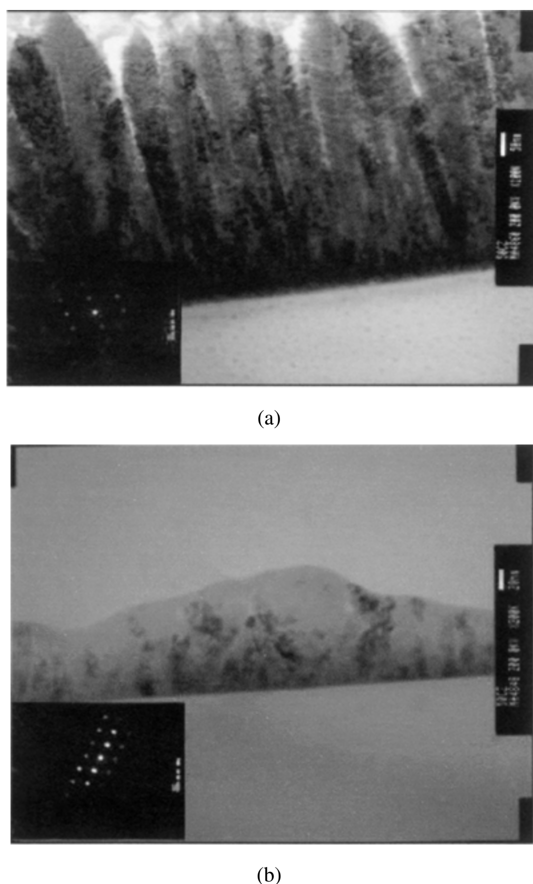

(a)

(b)

Fig. 4. TEM cross-sectional images and diffraction patterns of annealed $(Ce_{1-x}Zr_x)O_2$ films on Si (100): (a) $(Ce_{0.5}Zr_{0.5})O_2$ film (Ce power of 50 W) and (b) $(Ce_{0.75}Zr_{0.25})O_2$ film (Ce power of 100 W).

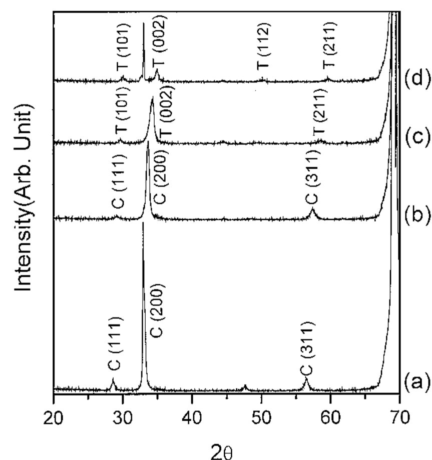

Fig. 5. XRD patterns of CeO_2 film and $(Ce_{1-x}Zr_x)O_2$ films annealed at 800°C deposited with different RF power of Ce: (a)–(d) are as in Fig. 3.

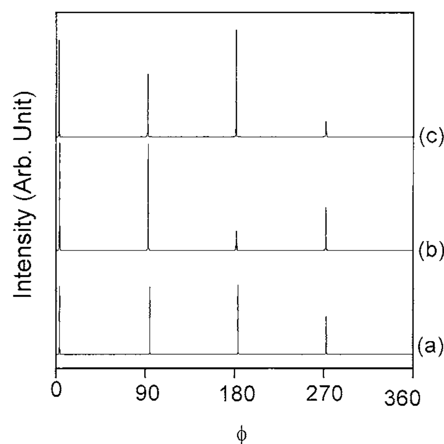

Fig. 6. X-ray ϕ scans of as-deposited $(Ce_{1-x}Zr_x)O_2$ films deposited on Si (100): (a) (220) scan of $(Ce_{0.75}Zr_{0.25})O_2$ film (100 W), (b) (112) scan of $(Ce_{0.5}Zr_{0.5})O_2$ film (50 W), and (c) (112) scan of $(Ce_{0.16}Zr_{0.84})O_2$ film (30 W).

a field emission source. The stoichiometry and thickness were analyzed by Rutherford backscattering spectrometry (RBS) using a 2 MeV tandem type ion accelerator. Auger electron depth profiles (AES, PHI-670, USA) with 4 KeV accelerating potential for Ar ion sputtering were used in order to investigate the Ni diffusion from the substrate into the buffer layer.

3. Results and Discussion

The deposition rate of $(Ce_{1-x}Zr_x)O_2$ films with each condition is shown in Fig. 2. It was observed that by increasing the RF power of the Ce target, the deposition rate was increased. When CeO_2 (RF, 100 W) or ZrO_2 (DC, 200 W) films were deposited separately at room temperature, each deposition rate was in the range of about 20–30 Å/min. However, when CeO_2 and ZrO_2 were co-deposited (Ce(RF, 30 W), Zr(DC, 200 W)), the deposition rate increased dramatically up to 125 Å/min. Furthermore, when the RF power of Ce was increased up to the 100 W level, the deposition rate of $(Ce_{1-x}Zr_x)O_2$ film was more than 10 times that of singly deposited CeO_2 or ZrO_2 films.

$(Ce_{1-x}Zr_x)O_2$ films ($0 \leq x \leq 0.84$) could be deposited simply by changing the RF power of the Ce target (Fig. 3). As-deposited ZrO_2 film was amorphous,

whereas as-deposited pure CeO_2 films (Fig. 3(a)) exhibited a cubic crystalline phase. The composition of each film was identically confirmed by both JCPDS data and RBS measurements and the crystal structures of the films corresponded well with the ZrO_2-CeO_2 phase diagram [13]. When the Zr target was co-sputtered with Ce, as-deposited $(Ce_{1-x}Zr_x)O_2$ film was also cubic crystalline phase, but the film had strong (002) texture, differing from that of pure CeO_2 (Fig. 3(b)). When Zr concentration in the film increased by reducing the power of the Ce target, the structure of as-deposited films changed to tetragonal with (002) texture (Fig. 3(c) and (d)). The TEM diffraction pattern of as-deposited $(Ce_{1-x}Zr_x)O_2$ films

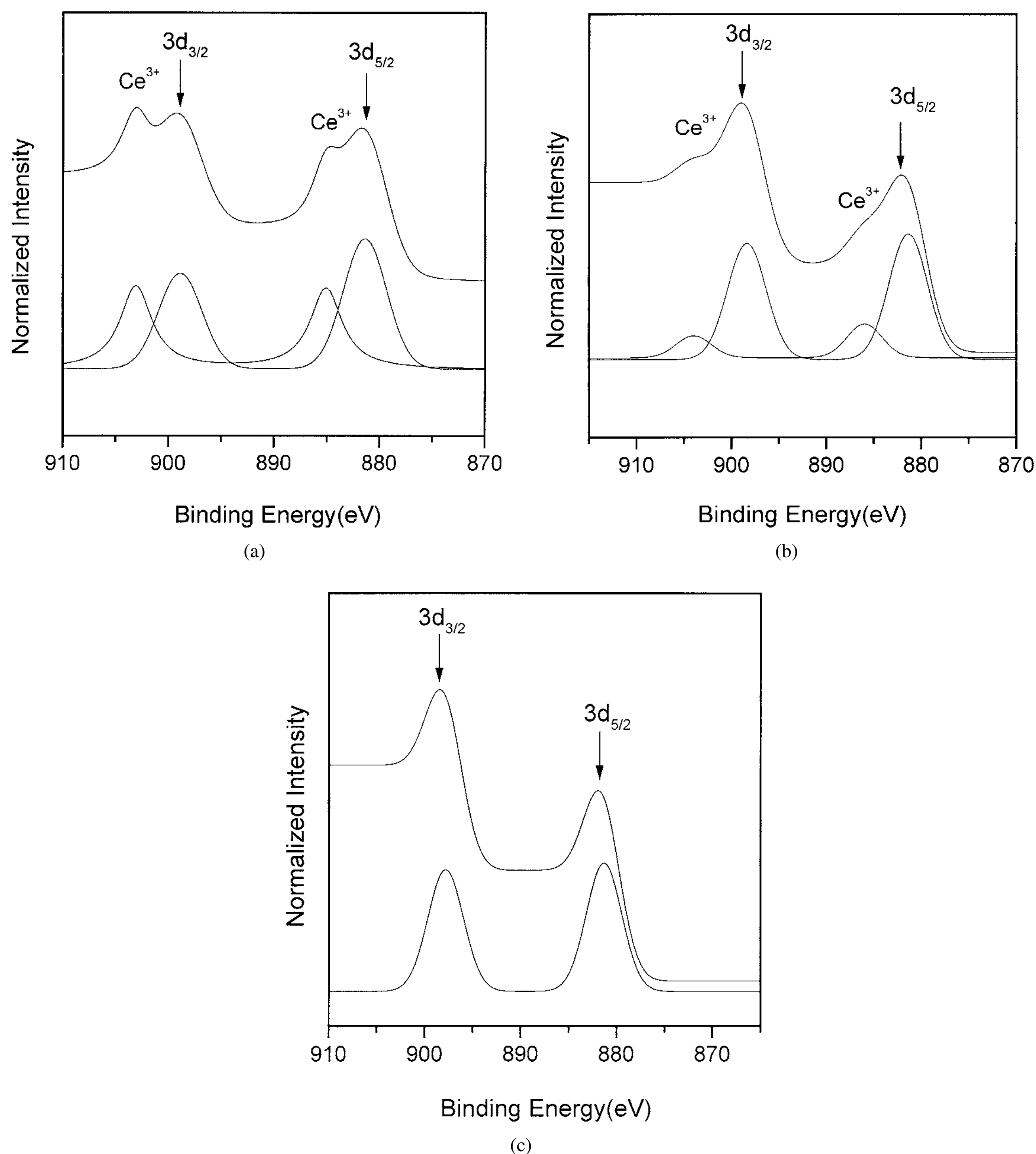

Fig. 7. XPS data for as-deposited $(Ce_{1-x}Zr_x)O_2$ films: (a) $(Ce_{0.16}Zr_{0.84})O_2$ film, (b) $(Ce_{0.5}Zr_{0.5})O_2$ film, and (c) $(Ce_{0.75}Zr_{0.25})O_2$ film.

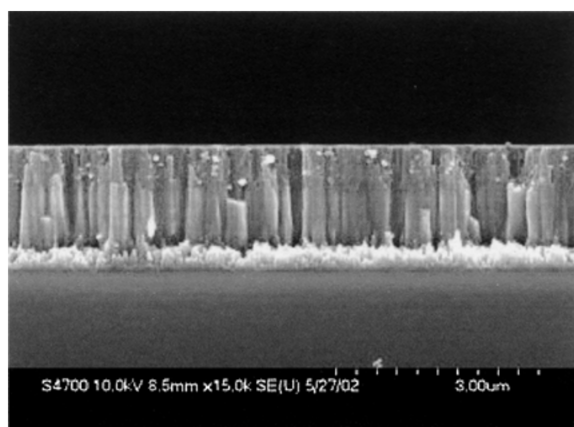

(a)

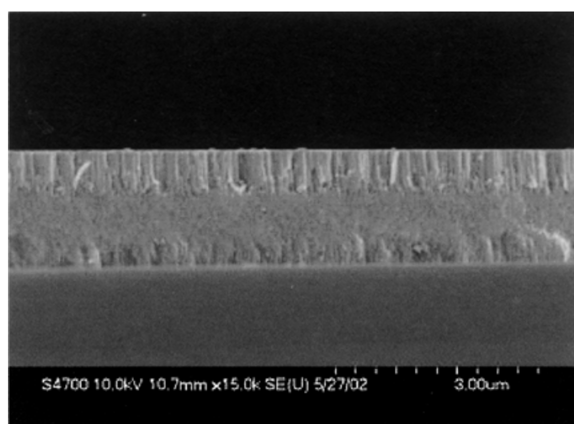

(b)

Fig. 8. SEM images of Si(100)(substrate)/CeO_2(200 nm)/($Ce_{0.75}Zr_{0.25}$)O_2(1100 nm)/($Ce_{0.5}Zr_{0.5}$)O_2(400 nm)/($Ce_{0.16}Zr_{0.84}$)O_2 (250 nm)/CeO_2(40 nm) buffer layer: (a) cross-section and (b) cross section annealed at 800°C.

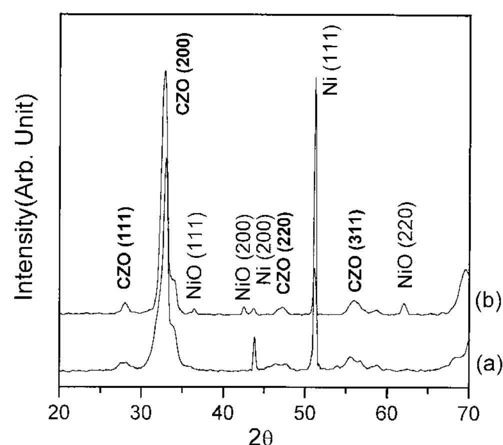

Fig. 9. XRD patterns of gradient ($Ce_{1-x}Zr_x$)O_2 films on polycrystalline Ni: (a) as-deposited film and (b) film annealed at 800°C.

confirmed the XRD data (Fig. 4); a diffraction pattern of ($Ce_{0.5}Zr_{0.5}$)O_2 film showed a tetragonal symmetry, while that of ($Ce_{0.75}Zr_{0.25}$)O_2 film showed a cubic symmetry. It was found that the specific texture did not change after annealing (Fig. 5). Figure 6 shows the four sharp diffraction peaks of the ϕ scans of ($Ce_{1-x}Zr_x$)O_2 films shown in Fig. 3. The XRD ϕ scans indicate that all mixed ($Ce_{1-x}Zr_x$)O_2 films grew biaxially on Si (100) substrates.

As shown in Fig. 7(a) and (b), the presence of Ce^{3+} was detected on both tetragonal ($Ce_{1-x}Zr_x$)O_2 films. However, Ce^{3+} was not detected in the cubic ($Ce_{0.75}Zr_{0.25}$)O_2 film (Fig. 7(c)). So, it was assumed that Ce^{3+} could stabilize tetragonal ZrO_2 films similar to Y^{3+} in YSZ. It seems that Ce^{3+} influences the stabilization of tetragonal ZrO_2 as well as the crystallization of ZrO_2 when its contents are relatively small, but at higher concentrations the role of CeO_2 was not a stabilizer in ZrO_2 but a component of cubic solid solution with ZrO_2.

($Ce_{1-x}Zr_x$)O_2 films with a concentration gradient of Ce could be obtained by varying the RF power of the Ce target during deposition without interrupting a batch sputtering procedure. A Si(100)(substrate)/CeO_2 (200 nm)/($Ce_{0.75}Zr_{0.25}$)O_2 (1100 nm)/($Ce_{0.5}Zr_{0.5}$)O_2 (400 nm)/($Ce_{0.25}Zr_{0.75}$)O_2 (250 nm)/CeO_2(40 nm) layered structure, was produced and is shown in Fig. 8. It was found that as-deposited film consisted of a dense and crack free columnar microstructure (Fig. 8(a)). When the film was annealed at 800°C simulating YBCO film deposition conditions, the ($Ce_{0.75}Zr_{0.2}$)O_2 layer changed into a denser structure (Fig. 8(b)). The same procedure was carried out using polycrystalline Ni substrate without a biaxially texturing, a commonly used material for YBCO-coated conductors. The XRD analysis showed that (200) c-axis textures, which are most suitable for textured YBCO, were sustained not only in as-deposited but also annealed films in which NiO has formed (Fig. 9). Figure 10 shows the Auger depth profiles for as-deposited and annealed buffer layers. It was found that the composition of Ce in the as-deposited film decreased successively with each buffer layer (Fig. 10(a)) and that Ni from substrate diffused into the ($Ce_{0.75}Zr_{0.25}$)O_2 layer during annealing (Fig. 10(b)). From the results, it was

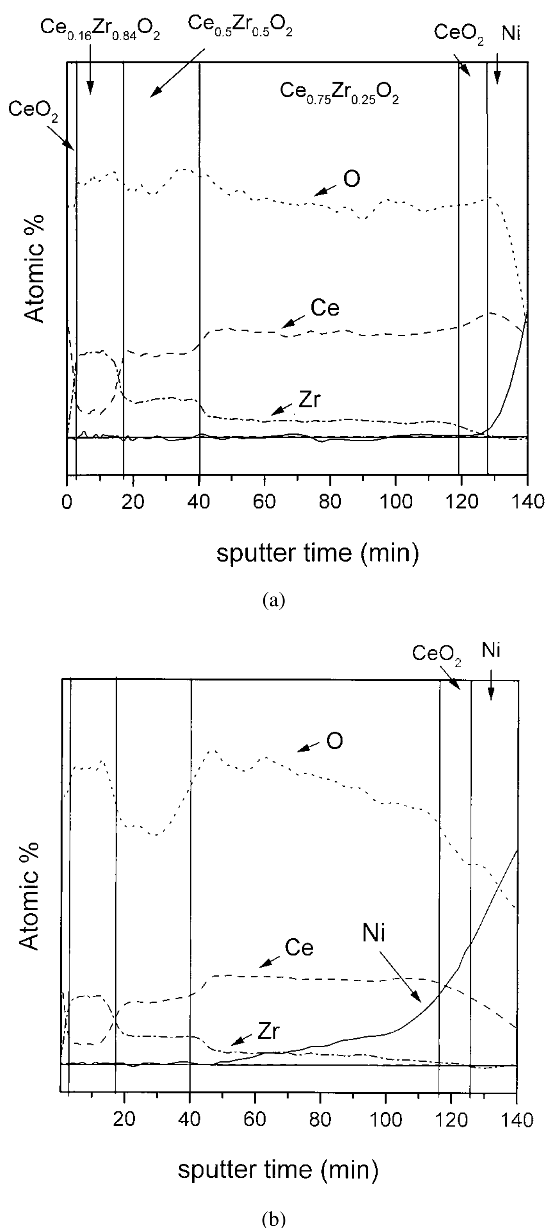

Fig. 10. Auger depth profiles of gradient $(Ce_{1-x}Zr_x)O_2$ films: (a) as-deposited and (b) annealed buffer layer.

confirmed that the role of $(Ce_{1-x}Zr_x)O_2$ layer was as a 'diffusion barrier' to Ni from the substrate.

4. Conclusions

$(Ce_{1-x}Zr_xO_2)$ films ($0 \leq x \leq 0.84$) were obtained by co-sputtering of Ce and Zr metal targets by varying RF power of the Ce target. When CeO_2 and ZrO_2 were co-deposited, the deposition rate was increased dramatically over that of single target sputtering. In particular, by increasing the Ce RF power to 100 W, the deposition rate of $(Ce_{1-x}Zr_x)O_2$ film was more than 10 times that of the CeO_2 and ZrO_2 films deposited separately. All as-deposited films containing Ce were crystalline and textured at room temperature. $(Ce_{0.16}Zr_{0.84})O_2$ film and $(Ce_{0.5}Zr_{0.5})O_2$ film, showed a tetragonal symmetry, while $(Ce_{0.75}Zr_{0.25})O_2$ film had a cubic symmetry. Therefore, it was concluded that low-level incorporation of Ce^{3+} could stabilize tetragonal ZrO_2 in the films just like Y^{3+} does in YSZ. However, in the case of $(Ce_{0.75}Zr_{0.25})O_2$ film, a cubic solid solution film was formed by co-sputtering. Compositional gradient $(Ce_{1-x}Zr_x)O_2$ films were deposited by varying the RF power of the Ce target during the sputtering process on Si(100) and polycrystalline Ni substrates. It was found that CZO($(Ce_{1-x}Zr_x)O_2$) films could be a potential buffer layer for HTSC films.

References

1. K. Chen, S. Afonso, Q. Xiong, G. Salamo, and F. Chan, *Physica C*, **282–287**, 613 (1997).
2. V. Vratskikh, Y. Drozdov, and V. Talanov, *Supercond. Sci. Technol.*, **10**, 766 (1997).
3. A. Goyal, D.P. Norton, J.D. Budai, M. Paranthaman, E.D. Specht, D.M. Kroeger, D.K. Cristen, Q. He, B. Smith, F.A. List, D.F. Lee, P.M. Martin, C.E. Klabunde, E. Hartfield, and V.K. Sikka, *Appl. Phys. Lett.*, **69**(12), 1975 (1996).
4. C.Y. Yang, S.E. Babcock, A. Goyal, M. Parathaman, F.A. List, D.P. Norton, D.M. Kroeger, and A. Ichinose, *Physica C*, **307**, 87 (1998).
5. D.F. Lee, M. Paranthaman, J.E. Mathis, A. Goyal, D.M. Kroeger, E.D. Specht, R.K. Williams, F.A. List, P.M. Martin, and C. Park, *Jpn. J. Appl. Phys.*, **38**, L178 (1999).
6. Y. Iijima, N. Tanabe, O. Kohno, and Y. Ikeno, *Appl. Phys. Lett.*, **60**, 769 (1992).
7. Y. Iijima, K. Onabe, N. Futaki, N. Yanabe, N. Sadakata, O. Kohno, and Y. Ikeno, *IEEE Trans. Appl. Supercond.*, **3**, 1510 (1993).
8. A.N. Khodan, J.P. Contour, D. Michel, O. Durand, R. Lyonnet, and M. Mihet, *J. Crystal Growth*, **209**, 828 (2000).
9. S. Rossignol, Y. Madier, and D. Duprez, *Catal. Today*, **50**, 261 (1999).
10. G. Colon, F. Valdivieso, M. Pijolat, R.T. Baker, J.J. Calvino, and S. Bernal, *Catal. Today*, **50**, 271 (1999).
11. N.M. Sammes, G.A. Tompsett, and Zhihong Cai, *Solid State Ionics*, **121**, 121 (1999).
12. E.N.S. Muccillo and D.M. Avila, *Ceramics International*, **25**, 345 (1999).
13. R.S. Roth, J.R. Dennis, and H.F. Mcmurdie, *Phase Diagrams for Ceramists*, **12**, 9946 (1987).